Peanut seeding depth control system based on MLE-KF and fuzzy PID control

Yan Yu[1,2,3], Yushuai Song[1,2,3], Xiaohong Liu[1,2,3*], Jiasheng Wang[1,2,3], Weikang Dong[1,2,3], Jun Liu[1,2,3], Yushuai Li[1,2,3]

(1. *College of Mechanical and Electrical Engineering, Qingdao Agricultural University, Qingdao 266109, Shandong, China*;
2. *Qingdao Plantech Mechanical Technology Co, Ltd, Qingdao 266109, Shandong, China*;
3. *Collaborative Innovation Center for Shandong's Main Crop Production Equipment and Mechanization, Qingdao 266109, Shandong, China*)

Abstract: Aiming at the problem that the consistency and stability of seeding depth are difficult to control during the complex field operation of peanut seeders, this study proposes a control method combining the Kalman Filter algorithm based on Maximum Likelihood Estimation (MLE-KF) and the Fuzzy PID algorithm. A system was designed to automatically adjust the furrow opener during the operation of the peanut seeder, thereby realizing the automatic control of seeding depth. This method maintains the peanut seeding depth within a reasonable error range suitable for growth, and effectively ensures the consistency of peanut seeding depth. In this study, displacement sensors and ultrasonic sensors were used to directly or indirectly detect the furrow depth. Combined with electric push rods and actuators, the furrow depth was adjusted in real time during the field operation of the peanut seeder. For the filtering fusion algorithm, a noise parameter adaptive algorithm based on sliding window and approximate MLE was adopted, while a Fuzzy PID control strategy was employed for the controller. Simulations were conducted in MATLAB/Simulink, and the simulation results showed that the improved algorithm achieved a significant improvement in seeding depth accuracy compared with the traditional Kalman Filter and PID control. Field tests were carried out with the qualification rate as the index under different operating speeds and seeding depth conditions. For this seeding depth control method, when the operation speed was 3 km/h and the furrow depth was set to 50.00 mm, the qualification rate of seeding depth reached 94.80%, with a standard deviation of 3.12 mm and a coefficient of variation of 6.08%. Compared with the traditional mechanical adjustment and passive adjustment methods, this method increased the qualification rate by 4.60% and 3.30%, respectively, and reduced the coefficient of variation by 2.46% and 3.01%, respectively. The research on the seeding depth control method in this study provides a new detection and control approach for the seeding depth control of peanut seeders.

Keywords: peanut seeder, seeding depth, MLE-KF, fuzzy PID, control system
DOI: 10.25165/j.ijabe.20261902.10374

Citation: Yu Y, Song Y S, Liu X H, Wang J S, Dong W K, Liu J, et al. Peanut seeding depth control system based on MLE-KF and fuzzy PID control. Int J Agric & Biol Eng, 2026; 19(2): 235–244.

1 Introduction

Peanut is an important oil crop and economic crop in China. Rational and efficient peanut cultivation is of great significance for ensuring the safety of edible oil, increasing agricultural efficiency, and improving farmers' production income[1,2]. Given the limited arable land, how to increase the per-mu yield of peanuts has become a key focus of current research[3]. The seeding depth of peanuts exerts a significant impact on improving the emergence rate and survival rate of seeds; therefore, controlling peanut seeding depth has become a critical factor for increasing peanut yield and accelerating economic growth[4,5]. However, there are relatively few studies on peanut seeding depth control at present, and the seeding depth control methods still remain at the traditional passive profiling methods such as fixed furrow openers or parallel four-bar linkages, which are unable to adjust the peanut seeding depth in real time during complex field operations[6,7]. Consequently, it is of great necessity and practical significance to study a seeding depth control system that can adjust the furrow depth in real time.

At present, the peanut seeding depth control in China has gradually transitioned from the traditional fixed furrow openers and passive profiling methods to active profiling that enables autonomous control of seeding depth. As scholars at home and abroad have deepened their research on seeding depth control, the focus of efforts to improve the consistency of peanut seeding depth has been placed on two aspects: measurement and execution[8]. In terms of seeding depth measurement, Liang et al.[9,10] proposed a seeding depth control device based on the collaboration of pressure

Received date: 2025-12-10 **Accepted date:** 2026-04-17
Biographies: Yan Yu, PhD, Professor, research interest: intelligent agricultural equipment, Email: 83518691@qq.com; **Yushuai Song**, MS candidate, research interest: agricultural electrification and automation, Email: 1006213566@qq.com; **Jiasheng Wang**, PhD, Professor, research interest: agricultural machinery and equipment, Email: jiasheng0813@163.com; **Weikang Dong**, MS candidate, research interest: agricultural engineering and information, Email: 18354673839@163.com; **Jun Liu**, MS candidate, research interest: agricultural machinery equipment engineering, Email: liuuu5980@163.com; **Yushuai Li**, MS candidate, research interest: agricultural machinery equipment engineering, Email: liyushuaili@163.com.
***Corresponding author: Xiaohong Liu**, PhD, research interest: intelligent agricultural equipment. College of Mechanical and Electrical Engineering. Qingdao Agricultural University, Qingdao 266109, China. Tel: +86-18300211266, Email: lxh964@126.com.

sensors and ultrasonic sensors. Zhao et al.[11,12] designed a seeder furrow depth control system based on displacement sensors, where Displacement Sensor Ⅰ and Displacement Sensor Ⅱ collect signals of the profiling wheel position and the hydraulic cylinder position stroke, respectively, to measure the seeding depth. Iqbal et al.[13,14] used ultrasonic sensors to obtain the height difference between the seed furrow and the frame, and realized real-time control of seeding depth through a microcontroller. Nielsen et al.[15,16] employed linear displacement sensors and ultrasonic sensors to measure the furrow opener depth and the distance between the frame and the soil surface, respectively. In terms of actuator control, Feng[17] designed a sliding knife-type furrow opener, and jointly controlled the seeding depth through a profiling mechanism and a depth-limiting wheel. Xue et al.[18] used an angle sensor to collect the angle of the swing arm when the post-seeding roller moves against the ground, and controlled the pre-seeding roller in real time through an electric cylinder to adjust the seeding depth—with the average seeding depth qualification rate reaching 93% at a speed of 3-5 km/h. Wang et al.[19,20] adopted a PLC as the main controller to control an electric push rod for adjusting the seeding depth. Zhao et al.[21] applied adaptive Kalman filtering based on a weighted average algorithm to filter and fuse the seeding depth data collected by laser sensors and ultrasonic sensors, and used a threshold control algorithm to control a servo electric cylinder for seeding depth regulation. By summarizing the above-mentioned experience and methods of seeding depth control, it can be concluded that the current research on peanut seeding depth control is relatively limited compared with that for other crops, and the seeding depth control accuracy is also relatively low. However, due to differences in seeding depth and planting spacing requirements, these existing methods cannot be directly applied to peanut cultivation. Furthermore, most of the current seeding depth control systems suffer from problems such as insufficient data acquisition accuracy and poor real-time performance[22-24]. Therefore, it is of great significance to study a seeding depth control system that features high data acquisition accuracy, strong real-time performance, and suitability for peanut characteristics.

Based on the planting characteristics of peanut ridge cultivation, an active seeding depth control system was designed, which integrates ultrasonic sensors and displacement sensors (with MLE-KF) for seeding depth data detection, and adopts an adaptive Fuzzy PID controller to regulate the electric actuator[25,26]. Aiming at the problems of traditional passive profiling (which is difficult to adapt to changes in complex field working environments) and conventional active profiling (such as insufficient data acquisition accuracy, outdated control strategies, and poor real-time performance), mathematical models for seeding depth detection, control, and execution were established[27,28].

2 Design of seeding depth control system for peanut seeder

2.1 Mechanical structure of seeding depth control system for peanut seeder

The seeding depth control system is mounted on the 1MB-2/4 peanut film-laying seeder produced by Qingdao Wannongda Peanut Machinery Co., Ltd. The mechanical structure of the system mainly consists of three parts: a detection mechanism, a data processing and control unit, and an execution mechanism (Figure 1).

The detection mechanism is composed of an ultrasonic sensor installed on the frame and a displacement sensor fixed on the cylinder of the electric push rod (for measuring the length of the electric push rod). The data processing and control unit consists of a control box with an STM32 microcontroller as its core. The execution mechanism includes an electric push rod, a parallel four-bar linkage, and a double-disc furrow opener.

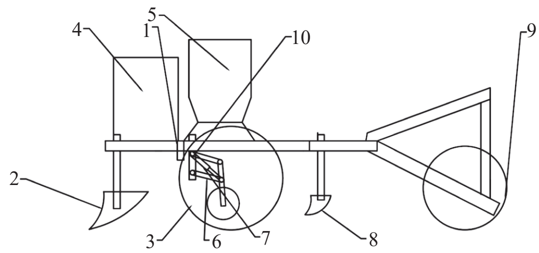

1. Ultrasonic sensor 2. Ridging device 3. Double-disc furrow opener 4. Control box 5. Seed box 6. Parallel four-bar linkage 7. Electric push rod 8. Soil covering device 9. Press wheel 10. Displacement sensor

Figure 1 Mechanical structure of peanut sowing depth control system

2.2 Working principle of the seeding depth control system

Before the sowing depth control system starts working, the sowing depth is determined according to the sowing environment, and the preset sowing depth value is set on the human-machine interface. During operation, the ultrasonic sensor and displacement sensor send the collected data to the STM32 microcontroller. The STM32 microcontroller performs filtering and fusion calculations on the data to obtain the estimated sowing depth, and adaptively adjusts the covariance based on historical data. The controller compares the estimated sowing depth with the preset value to calculate the deviation and deviation change rate, and obtains the control quantity of the electric push rod after processing by the fuzzy controller. Subsequently, the STM32 microcontroller controls the telescopic movement of the electric push rod according to the control quantity, which drives the double-disc furrow opener to move up and down through the parallel four-bar linkage until the sowing depth reaches the preset value. The working principle is shown in Figure 2.

2.3 Hardware design of seeding depth system

The seeding depth control system of this peanut seeder is centered on the STM32H743VIT6 microcontroller and mainly consists of four modules. The seeding depth detection module is composed of an HC-SR04 ultrasonic sensor with temperature compensation and a KTC-50 displacement sensor; the execution module adopts an XTL100 electric push rod, which is controlled by an L298N driver chip; the core control module is formed by the microcontroller equipped with a dual-channel power supply, a reset circuit, and a clock circuit; the human-machine interaction (HMI) module uses an HMI touchscreen for parameter adjustment and system status display. Since the microcontroller can only receive TTL signals, an RS485-to-TTL module is required for RS485 communication between the sensors and the microcontroller to realize signal conversion.

2.4 Establishment of the mathematical model for seeding depth control

Considering that the elastic deformation of ridge-tilled soil is less than 2%, the opener-soil system is simplified to rigid body motion, as shown in Figure 3. A coordinate system is established with point A as the origin, where the origin is the intersection of the longitudinal symmetry plane of the frame and the suspension point. Points A, B, C, D, E, F, G and angle α are as shown in Figure 3.

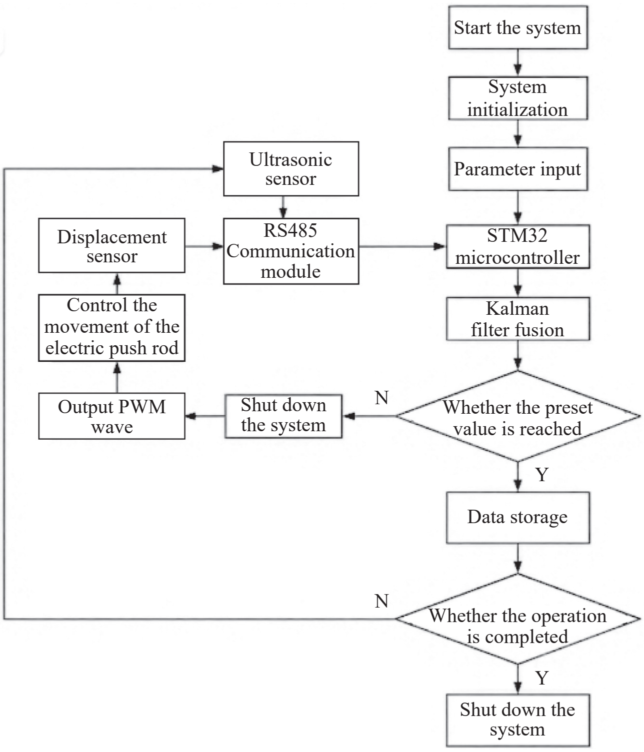

Figure 2 Schematic diagram of the seeding depth control system

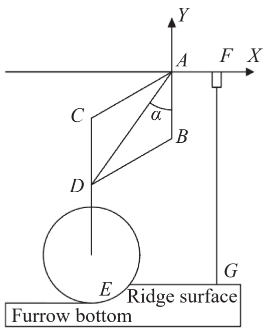

Note: *A*: The upper fixed hinge point of the parallel four-bar linkage and the frame, which is also the rear fixed point of the electric push rod. *B*: The lower fixed hinge point of the parallel four-bar linkage and the frame. *D*: The fixed hinge point of the parallel four-bar linkage and the furrow opener, as well as the front fixed point of the electric push rod. *E*: The lowest point of the disc edge of the double-disc furrow opener. *F*: The fixed point of the ultrasonic sensor on the frame. *G*: The measurement point of the ultrasonic sensor on the ridge surface. *α*: The included angle between the electric push rod and the frame, i.e., ∠BAD.

Figure 3 Schematic diagram for seeding depth calculation

The long side *AC* of the parallel four-bar linkage is 250 mm, and the short side *AB* is 150 mm. Since the peanut seeding depth is approximately 50 mm, which falls into the category of shallow seeding, and the double-disc furrow opener needs frequent adjustment during the seeding depth control process, a small-sized double-disc furrow opener with a disc diameter of 200 mm is selected. This selection aims to avoid reduced seeding depth control accuracy caused by an excessively large furrow opener and facilitate adjustment. The distance from the lower fixed hinge point *D* of the parallel four-bar linkage to the bottom of the double-disc furrow opener is 220 mm.

The ultrasonic sensor features a simple structure and strong penetration, and is used to measure the distance from the frame to the ridge surface. However, ultrasonic sensors may produce errors when the temperature changes, so an ultrasonic sensor with temperature compensation must be selected. Since the measurement range is within 1 m (a relatively short distance) and the soil becomes relatively soft after peanut ridges are formed, it is decided not to use a reflector. Instead, the probe directly emits ultrasonic waves to the ridge surface in front of the furrow opener to measure the vertical distance between the ultrasonic sensor point *F* and the ridge surface point *G* in front of the furrow opener.

$$d_u = \frac{c \cdot t}{2} \tag{1}$$

where, *c* is the propagation speed of ultrasonic waves in air varying with temperature, m/s; *t* is the round-trip time of ultrasonic waves from emission to reception of the reflected wave, s. The displacement sensor measures the length of *AD*, i.e., the length of the electric push rod is *L*. Through calculation, the angle of $\angle BAC$ can be obtained:

$$\alpha = \arccos\left(\frac{AB^2 + AD^2 - BD^2}{2AB \cdot AD}\right) \tag{2}$$

From this, the vertical distance *h* from the frame to the furrow bottom can be calculated using the angle *α*, the length *L* of the electric push rod, and the distance d_0 from the lower fixed hinge point of the electric push rod to the furrow bottom:

$$d_c = L \cdot \cos\alpha + d_0 \tag{3}$$

When calculating the furrowing depth, if only the displacement sensor is used to calculate the distance from the frame to the furrow bottom, large errors in the furrowing depth will occur when the ridge surface is uneven or the frame is tilted. Therefore, an ultrasonic sensor is used to detect the real-time distance from the frame to the ridge surface, eliminating the cumulative error caused by frame tilting. The furrowing depth is then calculated using the height difference between “frame to ridge surface” and “frame to furrow bottom”. At the current moment, this height difference is the theoretical furrowing depth:

$$h = d_c - d_u \tag{4}$$

By substituting the calculation expressions of the ultrasonic sensor and the displacement sensor, the expression for the theoretical furrowing depth is obtained:

$$h = L \cdot \frac{AB^2 + AD^2 - BD^2}{2AB \cdot AD} + d_0 - \frac{c \cdot t}{2} \tag{5}$$

After Equation (5) is calculated by the microcontroller, the obtained *h* is compared with the set furrowing depth h_0:

If $h<h_0$ (the furrowing depth is too shallow), the microcontroller controls the motor to rotate forward, extending the electric push rod to increase the furrowing depth until the set furrowing depth is met.

If $h>h_0$ (the furrowing depth is too deep), the microcontroller controls the motor to rotate in reverse, retracting the electric push rod to reduce the furrowing depth until the set furrowing depth is met.

If $h=h_0$ (the furrowing requirement is satisfied), the microcontroller outputs no signal and the electric push rod remains inactive.

2.5 Design of seeding depth adjustment mechanism

The seeding depth adjustment mechanism uses a parallel four-bar linkage as the motion transmission carrier and an electric push rod as the power source. Through the parallel four-bar linkage, the linear telescopic motion of the electric push rod is converted into the vertical lifting motion of the furrow opener, ensuring that the furrow opener blade E always enters the soil vertically.

2.5.1 Load analysis of seeding depth adjustment mechanism

Most researchers, when conducting studies on seeding depth control, often adopt a hydraulic system for the seeding depth adjustment mechanism, considering the large load of the parallel four-bar linkage during field operations and high soil resistance. However, the hydraulic system has slow adjustment speed and relatively poor real-time performance. Therefore, this study uses an electric push rod to address the issue of real-time performance. Since the output force of the electric push rod is far less than that of the hydraulic system, the load issue needs to be considered:

When the peanut seeder operates stably, only static loads need to be considered. These mainly include the furrow opener's soil penetration resistance, the mechanism's gravity, and the hinge friction. The equation is as follows:

$$F_{\text{static}} = F_{\text{soil}} + G_{\text{total}} \cdot \sin\theta + F_{\text{friction}} \quad (6)$$

where, F_{soil} is soil penetration resistance of the double-disc furrow opener, N; F_{total} is total gravity of the parallel four-bar linkage and the furrow opener, N; F_{friction} is sliding friction force at the hinge points, N.

When the seeding depth changes, the electric push rod drives the parallel four-bar linkage to generate dynamic loads due to inertia force during the adjustment process. According to Newton's second law, the calculation Equation is as follows:

$$F_{\text{dynamic}} = m_{\text{total}} \cdot a_D \quad (7)$$

where, m_{total} is total mass of the parallel four-bar linkage and the furrow opener, kg; $a_D = d^2x_D/dt^2$ represents horizontal acceleration of hinge point D, m/s^2.

The force transmission ratio of the parallel four-bar linkage is iF=cosα, where α is the angle between the electric push rod and the vertical direction. Therefore, the equivalent load of the mechanism can be calculated as follows:

$$F_{\text{eq}} = \frac{F_{\text{static}} + F_{\text{dynamic}}}{iF} \quad (8)$$

Combined with Equation (8), the output force of the electric push rod must cover static load + dynamic load + sudden changes in soil resistance, and its Equation is as follows:

$$F_{\text{push}} \geq k_F \cdot F_{\text{eq}} \quad (9)$$

where, k_F is the safety margin.

2.5.2 Dynamic model of electric push rod-four-bar linkage

The dynamic response of the electric push rod directly determines the real-time performance and precision of seeding depth adjustment for the peanut seeder. By integrating the basic model of the electric push rod with the equivalent load of the parallel four-bar linkage, a linked dynamic model covering motor drive, mechanical transmission, and load response is established. The motor drive model adopts the armature voltage balance equation of the brushed DC motor:

$$U = R_a i_a + L_a \frac{di_a}{dt} + K_e\omega + E_{\text{load}} \quad (10)$$

where, R_a is armature winding resistance, Ω; i_a is armature current, A; L_a is armature winding inductance, H; $L_a di_a/dt$ represents armature inductive voltage drop, V; K_e is back electromotive force (EMF) constant, V/rad·s^{-1}; ω is motor armature angular velocity, rad/s; E_{load} is load additional electromotive force, V.

The mechanical transmission model: The motor torque is transmitted to the parallel four-bar linkage through the speed reduction mechanism and the lead screw. The relationship among its rotational speed, displacement, and force is as follows: the relationship between the motor angular velocity and the telescopic speed of the push rod:

$$\frac{dL}{dt} = \frac{\omega \cdot L_{\text{gear}}}{2\pi \cdot i_{\text{gear}}} \quad (11)$$

where, i_{gear} is the reduction ratio of the electric push rod, and L_{gear} is the lead of the lead screw, m/r.

The relationship between the motor torque and the output force of the push rod:

$$T_e = \frac{F_{\text{eq}} \cdot L_{\text{gear}}}{2\pi \cdot i_{\text{gear}} \cdot \eta} \quad (12)$$

where, η represents the mechanical transmission efficiency, and T_e represents the motor electromagnetic torque, N·m.

By combining Equations (10)-(12), the differential equation of the electric push rod's telescopic displacement L with respect to time t can be obtained:

$$\frac{d^2L}{dt^2} + \frac{R_a \cdot 2\pi i_{\text{gear}}}{K_t K_e \eta L_{\text{gear}}} \cdot \frac{dL}{dt} + \frac{2\pi i_{\text{gear}} \cdot E_{\text{load}}}{K_t K_e \eta L_{\text{gear}}} = \frac{U \cdot 2\pi i_{\text{gear}}}{K_t K_e \eta L_{\text{gear}}} \quad (13)$$

This equation represents a second-order linear system. Through calculations, its damping ratio $\xi \approx 0.70$ and natural frequency $\omega_n \approx 10.2$ rad/s are obtained, which meet the requirements of no overshoot and fast response for field operations.

2.5.3 Quantitative calculation of seeding depth adjustment and electric push rod output

Based on the mapping relationship between h and L in Equation (5), the quantitative relationships between the seeding depth adjustment and the electric push rod output (i.e., telescopic stroke and output force) are derived through incremental analysis, which can be directly used for the issuance of control commands.

When the ridge height YG remains approximately unchanged during short-term adjustment, increments are taken on both sides of Equation (5). Under the condition that the ridge height YG remains approximately unchanged during short-term adjustment, increments are taken on both sides of Equation (5). To simplify the calculation while meeting the accuracy requirement and under the condition that $\Delta L \ll L$, high-order small terms are ignored, and the simplified result is obtained as follows:

$$\Delta h \approx \frac{(BD - AB) \cdot \frac{\sqrt{L^2 - AB^2}}{BD^2} \cdot \Delta L}{\sqrt{1 - \left(\frac{\sqrt{L^2 - AB^2}}{BD^2}\right)}} \quad (14)$$

Combined with the initial state, after substituting L=L_0, it is further simplified into a linear mapping relationship:

$$\Delta h = k_{hL} \cdot \Delta L \quad (15)$$

where, k_{hL} is the mapping coefficient between the seeding depth and the telescopic stroke of the electric push rod.

When a peanut seeder is operating in the field, if the actual seeding depth decreases due to uneven ridge surfaces or changes in soil resistance, it needs to be adjusted to the target seeding depth. The calculation process is as follows:

$$\Delta h = h_{\text{target}} - h_1 \quad (16)$$

Substitute Equation (16) into Equation (17) to calculate the telescopic stroke of the electric push rod, and the final length of the electric push rod is obtained through calculation:

$$L_{\text{final}} = L_0 \pm \left| \frac{\Delta h}{k_{hL}} \right| \quad (17)$$

Meanwhile, the motor armature current corresponding to the output force of the electric push rod is:

$$i_a = \frac{F_{\text{push}} \cdot 2\pi i_{\text{gear}} \cdot \eta}{K_t \cdot L_{\text{gear}}} \quad (18)$$

Finally, the command voltage is obtained from the mapping relationship between output force and voltage, which is then converted into the PWM duty cycle D. The Equation is as follows:

$$D = D_0 + \frac{U}{U_{\max}} \cdot (D_{\max} - D_0) \quad (19)$$

where, D_0 is the zero-action duty cycle, %; $U_{\max}$ is the rated voltage of the electric push rod, V; and $D_{\max}$ is the maximum duty cycle, %.

2.6 Kalman filtering algorithm based on maximum likelihood estimation

During the field operation of the peanut seeder, the ultrasonic sensor will inevitably produce data anomalies due to the complexity of the operating environment and the machine's own vibration. Additionally, the sensor generates noise during its operation. These factors will cause significant errors in the seeding depth data collected by the sensor, thereby affecting the control of seeding depth. Therefore, it is necessary to select an effective filtering and fusion algorithm to eliminate outliers and reduce the interference of noise.

The Kalman filter features high computational efficiency, low complexity, and explicit noise handling. It can effectively address noise and anomalies during sensor detection, making it highly suitable for data filtering and fusion of the peanut seeder's multi-sensor system. To better adapt to the field operation environment, the original Kalman filter algorithm was studied, and a Kalman filter algorithm based on maximum likelihood estimation was proposed. By adaptively estimating the key noise parameters (measurement noise covariance R) in the Kalman filter, this algorithm solves the problem that the traditional Kalman filter relies on prior knowledge of noise parameters and is difficult to adapt to complex environments.

2.6.1 Construction of MLE-KF system model

Taking the theoretical ditching depth h in Equation (5) as the core state variable, a discrete-time system model is constructed. Considering the continuity of velocity variation when the electric linear actuator drives the ditching device to move up and down, the sowing depth h and its rate of change are adopted as state variables to reflect the moving speed of the ditching device, thereby constructing a two-dimensional state vector as follows:

$$x(k) = \begin{bmatrix} h(k) \\ \dot{h}(k) \end{bmatrix} \quad (20)$$

The state equation is as follows:

$$x(k) = Ax(k-1) + \omega(k-1) \quad (21)$$

Among them, $A = \begin{bmatrix} 1 & \Delta t \\ 0 & 1 \end{bmatrix}$ is the state transition matrix; Δt is the sampling period; $\omega(k) \sim N(0, Q)$ is the process noise.

The measurement equation is as follows:

$$z(k) = Hx(k) + v(k) \quad (22)$$

The measurement vector $z(k) = h_{\text{raw}}(k)$, i.e., the theoretical furrowing depth calculated by Equation (5); the measurement matrix $H = [1\ 0]$; the measurement noise $v(k) \sim N(0, R)$, which reflects the cumulative effect of sensor noise.

2.6.2 Adaptive noise parameter estimation based on sliding window and approximate MLE

In the process of seeding depth control for peanut seeders, ensuring the real-time performance of the system is of paramount importance. The traditional Maximum Likelihood Estimation (MLE) algorithm calculates the likelihood function using all historical data and employs the gradient descent method for iterative solutions, which results in a large computational load and makes it unsuitable for embedded systems. To enhance the real-time performance of the system, this study simplifies the traditional MLE algorithm by adopting a fixed-length sliding window to store historical data and using an analytical approximation method to directly compute the covariance, thereby avoiding the complex iterative optimization process.

Sliding Window Method: First, a sliding window with a length of N (where N=100) is set to store the measurement residuals and their corresponding residual covariances at the latest N time instants. When the system starts, the initially set measurement noise covariance R is used for the first N time instants. After N time instants, the measurement noise covariance R is adaptively updated using the sample variance of the first N normal sampling data, while the process noise covariance Q is set to a fixed value. At the k-th time instant, after completing the prediction and update steps of the Kalman filter, the measurement residual and residual covariance at the current time instant are stored in the sliding window, and the oldest data in the window is removed, ensuring that the window always contains the latest N sets of data[29].

Approximate MLE for updating measurement noise covariance R: Since the movement state of the peanut seeder changes slowly during field operations, the process noise covariance Q is kept fixed to simplify calculations. During system operation, the measurement noise covariance R is not updated at every step; instead, a low-frequency triggering mechanism is adopted. R is re-estimated only every 100 sampling periods or when the mean value of measurement residuals in the sliding window changes significantly[30]. When the conditions for updating R are met, based on the N sets of data $\{d_i, S_i\}$ $(i = k-N+1, k-N+2, \ldots, k)$ in the sliding window, the approximate maximum likelihood estimate of the measurement noise covariance R is calculated using the following analytical Equation:

$$\hat{R} = \frac{1}{N} \sum_{i=k-N+1}^{k} \left(d_i d_i^{\mathrm{T}} - S + Q \right) \quad (23)$$

where, $\hat{R}$ is the approximate maximum likelihood estimate of the measurement noise covariance; d_i is the measurement residual at i-th time instant; S_i is the residual covariance matrix at the i-th time instant.

This method utilizes the statistical characteristics of the residual d_i, approximates the expectation with the sample mean of the N sets of data in the sliding window, and directly obtains the analytical solution of R. It avoids the iteration of the gradient descent method, significantly reduces the computational load, and meets the high real-time requirements of the STM32 microcontroller.

2.6.3 Seeding depth data fusion

Based on the optimal estimation at the previous time instant, the current state is predicted as follows:

$$\hat{x}(k|k-1) = A\hat{x}(k-1|k-1) \quad (24)$$

$$P(k|k-1) = AP(k-1|k-1)A^{\mathrm{T}} + Q \quad (25)$$

The initial state is $\hat{x}(0|0) = \begin{bmatrix} h_0 \\ 0 \end{bmatrix}$, and the initial covariance is

$P(0|0) = diag([20, 10])$.

The Kalman gain is calculated based on the predicted value as follows:

$$K(k) = \frac{P(k|k-1)H^{\mathrm{T}}}{HP(k|k-1)H^{\mathrm{T}} + \hat{R}} \tag{26}$$

Revise the state estimation:

$$\hat{x}(k|k) = \hat{x}(k|k-1) + K(k) \cdot v(k) \tag{27}$$

Update the covariance matrix:

$$P(k|k) = (1 - K(k)H)P(k|k-1) \tag{28}$$

Finally, the fused seeding depth estimation value $\hat{h}(k) = \hat{x}_1(k|k)$ is output, which serves as the input for the subsequent fuzzy PID control.

2.7 Design of adaptive fuzzy PID control system

As shown in Figure 4, the adaptive fuzzy PID consists of two parts: a conventional PID controller and a fuzzy reasoning regulator. The adaptive fuzzy PID controller dynamically modifies PID parameters through fuzzy reasoning to achieve precise control of seeding depth, addressing the issue that traditional PID has insufficient adaptability to disturbances such as sudden changes in field soil resistance and frame vibration. The algorithm is optimized from four dimensions: variable fuzzification, fuzzy reasoning rules, defuzzification methods, and parameter self-tuning, to ensure the real-time performance and accuracy of seeding depth control during peanut sowing operations.

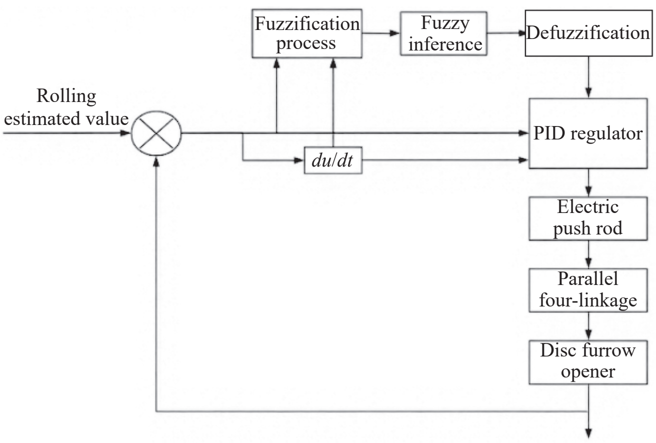

Figure 4 Schematic diagram of seeding depth controller structure

2.7.1 Structure of the adaptive fuzzy PID controller

The controller forms a closed-loop control system consisting of a conventional PID module and a fuzzy reasoning regulator. The input layer controller reads the fused seeding depth estimation value $\hat{h}(k)$ output by MLE-EF. The control system then compares this seeding depth estimation value with the preset seeding depth value, and calculates the deviation $e(k)$ and the deviation change rate $e_c(k)$.

$$\begin{cases} e(k) = h_0 - \hat{h}(k) \\ e_c(k) = \dfrac{e(k) - e(k-1)}{\Delta t} \end{cases} \tag{29}$$

In the fuzzy reasoning layer, the seeding depth control system performs fuzzification on input variables e and e_c to obtain fuzzy variables E and E_c. A fuzzy rule table was established based on expert experience and the dynamic characteristic requirements of seeding depth control. The seeding depth controller conducts fuzzy reasoning and defuzzification on fuzzy variables E and E_c. According to the fuzzy rule table, the rules are activated through maximum membership degree matching, and the correction ΔK_p, ΔK_i, ΔK_d for PID parameters is output.

The PID execution layer calculates the control quantity u based on the corrected parameters, converts it into a PWM signal to drive the electric push rod, and drives the electric push rod to adjust the height of the furrow opener, thereby realizing the closed-loop control of seeding depth.

2.7.2 Design of variable fuzzification

The purpose of fuzzification is to convert the precise seeding depth deviation and deviation change rate into fuzzy linguistic variables. Combined with the agronomic requirements for peanut seeding depth, the basic universe of discourse, quantitative universe of discourse, and quantization factors of the variables are optimized.

According to the field operation test of the peanut seeder, the maximum fluctuation range of seeding depth deviation is [–5, 5], and the deviation change rate is [–4, 4]. Seven fuzzy subsets are set: NB (Negative Big), NM (Negative Medium), NS (Negative Small), ZO (Zero), PS (Positive Small), PM (Positive Medium), and PB (Positive Big). These fuzzy subsets are quantified into a universe of discourse, as listed in Table 1.

Table 1 Fuzzy PID parameter settings

Basic variable	e	e_c	ΔK_p	ΔK_i	ΔK_d
Fuzzy variable	E	E_c	ΔK_p	ΔK_i	ΔK_d
Fuzzy subset	[NB NM NS ZO PS PM PB]				
Quantized universe of discourse	[–5, 5]	[–4, 4]	[–0.8, 0.8]	[–0.06, 0.06]	[–1.0, 1.0]

During the operation of the system, there are high requirements for real-time performance. To facilitate implementation, an equally divided triangular membership function is adopted, as it involves low computational complexity and is suitable for real-time control. This function is shown in Figure 5.

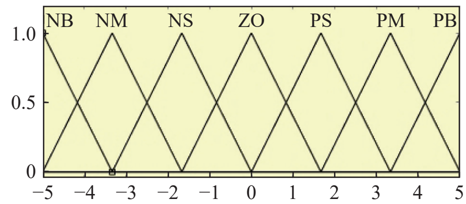

Figure 5 Triangular membership function of seeding depth deviation e

2.7.3 Design of fuzzy inference rules

Fuzzy rules were established based on field operation requirements and expert experience through field tests and professional analysis. The core logic is as follows:

When the seeding depth deviation is large, priority is given to increasing K_p to quickly eliminate the deviation, reducing K_i to avoid overshoot, and increasing K_d to suppress disturbances.

When the deviation is moderate, moderately reduce K_p, increase K_i to eliminate steady-state errors, and keep K_d at a medium level.

When the deviation is small or non-existent, reduce K_p to prevent oscillation, increase K_i to stabilize the seeding depth, and adjust K_d according to the deviation change rate. Based on experimental data analysis and professional technical experience, a fuzzy rule table was established as listed in Table 2. The fuzzy control rules are input into Matlab, and the resulting rule cloud diagrams of the fuzzy controller are shown in Figure 6.

Table 2 Fuzzy control rule table

e	e_c						
	NB	NM	NS	ZO	PS	PM	PB
NB	PB/NB/PS	PB/NB/NS	PM/NM/NB	PM/NM/NB	PS/NS/NB	ZO/ZO/NM	ZO/ZO/PS
NM	PB/NB/PS	PB/NB/NS	PM/NM/NB	PS/NS/NM	PS/NS/NM	ZO/ZO/NS	NS/ZO/ZO
NS	PM/NM/ZO	PM/NM/NS	PN/NS/NM	PS/NS/NM	ZO/ZO/NS	NS/PS/NS	NS/PS/ZO
ZO	PM/NM/ZO	PM/NS/NS	PS/NS/NS	ZO/ZO/ZO	NS/PS/PS	NM/PS/PS	NM/ZO/PM
PS	PS/ZO/NS	PS/ZO/NS	ZO/ZO/ZO	NS/PS/PS	NS/PS/PS	NM/PM/PM	NM/PM/PM
PM	PS/PS/ZO	ZO/ZO/ZO	NS/PS/PS	NM/PM/PS	NM/PM/PM	NM/PB/PB	NB/PS/PB
PB	ZO/PB/ZO	ZO/PM/ZO	NM/PM/PS	NM/PM/PM	NM/NB/PM	NB/PS/PB	NB/PB/PB

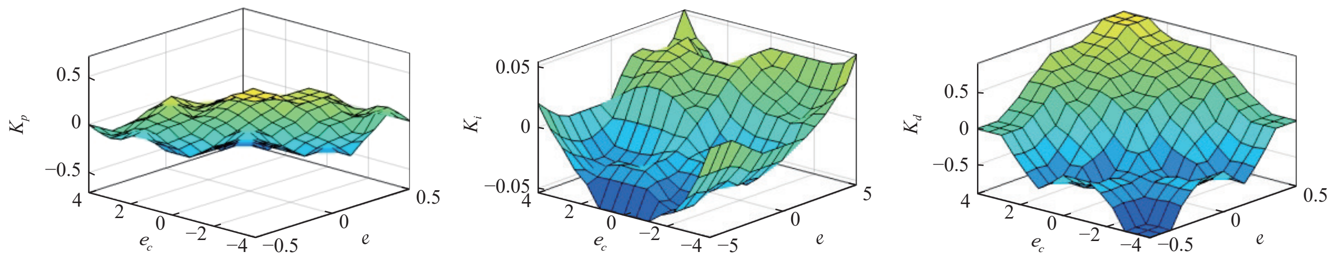

a. K_p fuzzy rules b. K_i fuzzy rules c. K_d fuzzy rules

Figure 6 Cloud diagrams of K_p, K_i, and K_d fuzzy rules

2.7.4 Defuzzification and parameter self-tuning

To make full use of information from all fuzzy subsets and avoid correction errors caused by a single subset, the center of gravity method is adopted for the defuzzification process of the peanut seeding depth controller. Taking ΔK_i as an example, its defuzzification equation is as follows:

$$\mu_{\Delta K_i} = \frac{\sum_{U_{\Delta K_i}} \mu_R(U_{\Delta K_i})U_{\Delta K_i}}{\sum_{U_{\Delta K_i}} \mu_R(U_{\Delta Ki})} \tag{30}$$

where, $\mu_R(U_{\Delta K_i})$ is the membership function of the fuzzy set of ΔK_i on the universe of discourse μ_R.

In the seeding depth controller, the real-time self-tuning Equation for its PID parameters is as follows:

$$\begin{cases} K_p = K_p' + \Delta K_p \\ K_i = K_i' + \Delta K_i \\ K_d = K_d' + \Delta K_d \end{cases} \tag{31}$$

Through the pre-experiment of peanut seeding depth in a flat field, the target seeding depth was set to 50 mm. After multiple adjustments, the initial reference values $K_p' = 2.5$, $K_i' = 1.6$, and $K_d' = 0.2$ were obtained.

3 Results

3.1 Simulation verification and analysis based on Matlab

To verify the advantages of the seeding depth control method based on the MLE algorithm and fuzzy PID control, a comparative simulation model of peanut seeding depth control was developed and built in Matlab-R2024b/Simulink, which was compared with the traditional Kalman filtering algorithm and traditional PID algorithm.

To obtain the measured seeding depth h calculated from the sensor data during peanut seeding, a sensor module is built in Simulink. Considering error factors such as field temperature variation and mechanical vibration of the seeder, the module adopts a multi-sensor fusion modeling method. Sine signals are used to simulate temperature interference on the ultrasonic sensor, combined sine signals and white noise to simulate mechanical vibration interference of the peanut seeder, and ramp signals to simulate the extension length of the electric push rod measured by the displacement sensor. As shown in Figure 7, the real-time seeding depth h is calculated and output according to the physical relationship between sensor parameters and seeding depth.

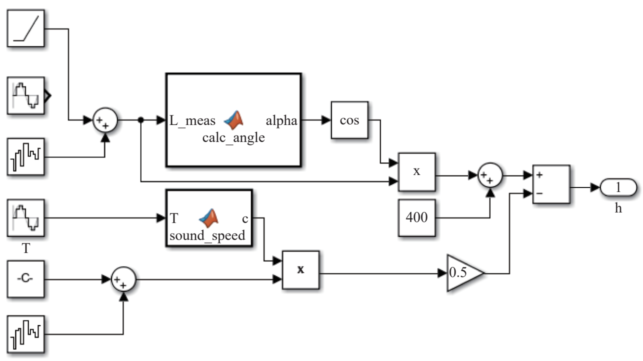

Figure 7 Simulation of simulink sensor module

In Simulink, the basic structure of the ordinary Kalman filter is first built, and then the MLE algorithm is introduced through the Matlab Function to optimize the noise covariance. The real-time seeding depth h output by the sensor module is processed by the ordinary Kalman filter and the Kalman filter based on the MLE algorithm respectively to obtain the seeding depth prediction value.

As can be seen from the figure, the Kalman filter based on the MLE algorithm can adaptively adjust the noise covariance. When the seeding depth changes drastically or the noise interference is large, its estimation curve is closer to the actual seeding depth, and both the smoothing effect and tracking accuracy are better than those of the ordinary Kalman filter.

To achieve precise control of seeding depth, a fuzzy PID controller is designed. The deviation is obtained by calculating the difference between the seeding depth estimation value (after Kalman filtering) and the seeding depth set value, and the deviation change rate is calculated. Both the deviation and its change rate are input into the fuzzy controller, which outputs the control quantity of the electric push rod.

By comparing the output value of the fuzzy PID with that of the traditional PID (as shown in Figure 8 and Figure 9), it can be found that the output curve of the traditional PID controller has obvious periodic fluctuations. In contrast, the output curve of the fuzzy PID controller is much smoother, with a stable rising process and no obvious oscillation.

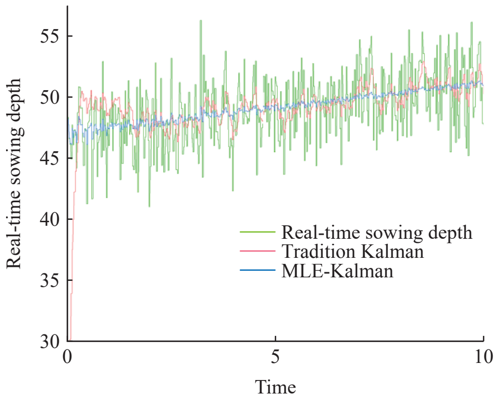

Figure 8 Comparison diagram of signal filtering

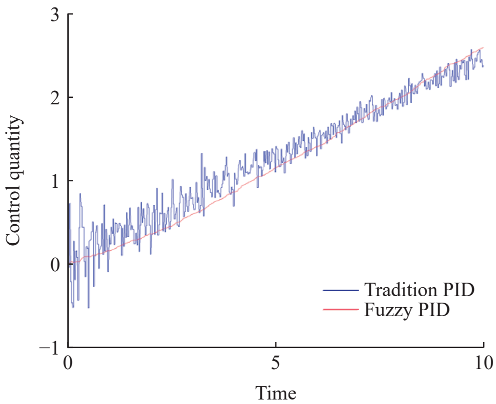

Figure 9 Comparison diagram of seeding depth control quantities

3.2 Field experiments

To verify the adaptability of the peanut seeding depth control system (integrating MLE-KF data fusion and fuzzy PID control) designed in this study under complex field operation conditions, as well as its seeding depth control accuracy, stability, and real-time performance at different seeding depths and operation speeds, field experiments were conducted using the 1MB-2/4 peanut film-laying seeder produced by Qingdao Wannongda Peanut Machinery Co., Ltd.

The experiments used "Silihong" peanut seeds and were carried out in September 2025 at the Teaching Experimental Base of Qingdao Agricultural University, Laixi City, Shandong Province, China. The test plot area was approximately 600 m^2, and rotary tillage was performed in advance to ensure uniform soil bulk density in the plot, avoiding test deviations caused by excessively hard or soft local soil[31]. The field experiments are shown in Figure 10.

Figure 10 Field experiment

To obtain more accurate field test data, the traditional control method was retained for the left and right outermost furrowing devices of the two-ridge, four-row seeder, while the two inner furrow openers were optimized. Based on GB/T 6973-2005 Test Methods for Single Seeders (Precision Seeders), gradient control tests were set up to measure the seeding depth qualification rate and depth variation coefficient.

3.2.1 Test method

To isolate the optimization effects of the MLE-KF filter and fuzzy PID, three control groups were set up in accordance with Shandong's peanut seeding standards. The control scheme with the MLE-KF + fuzzy PID algorithm served as the experimental group, the traditional passive profiling control scheme as Control Group 1, and the mechanical adjustment control scheme as Control Group 2.

Tests were conducted for three seeding depths (40 mm, 50 mm, 60 mm) and three operation speeds (3 km/h, 4 km/h, 5 km/h) respectively. According to the agronomic requirements for shallow peanut seeding, the allowable error for qualified seeding depth is ±5 mm.

The ground surface height was calibrated, and soil was scraped to expose the peanut seeds to measure the distance between the seeds and the ground surface. Five experimental subgroups were set up for measurement, with the seeder traveling one round trip in each subgroup. The test data are shown in Figure 11.

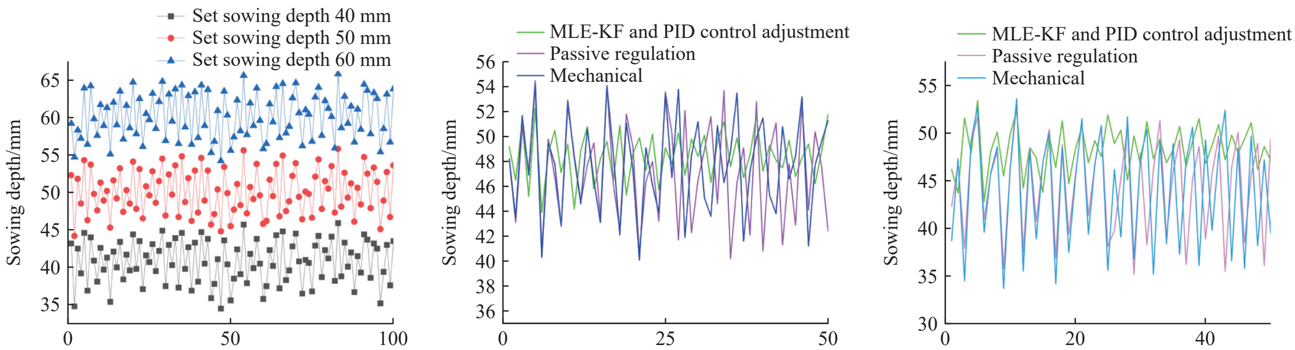

a. Active adjustment method with different seeding depths set at 3 km/h

b. Three seeding depth adjustment methods when the seeding depth is set to 50 mm and the speed is 4 km/h

c. Three adjustment methods when the seeding depth is set to 50 mm and the speed is 5 km/h

Figure 11 Field data diagrams

3.2.2 Calculation of test results

Based on the data obtained from the tests, the average seeding depth, seeding depth qualification rate, standard deviation, and coefficient of variation were calculated for the traditional mechanical adjustment, passive adjustment, and active adjustment under different operation speeds and different set depths. The calculation Equations are as follows:

$$\bar{h} = \frac{\sum_{i=1}^{N} h_i}{N} \tag{32}$$

$$P = \frac{n}{N} \times 100\% \tag{33}$$

$$S = \sqrt{\frac{\sum_{i=1}^{N} \left(h_i - \bar{h}\right)^2}{N-1}} \tag{34}$$

$$\mathrm{CV} = \frac{S}{\bar{h}} \times 100\% \tag{35}$$

where, $\bar{h}$ represents the average seeding depth, m; P represents the seeding depth qualification rate, %; S represents the seeding depth standard deviation, m; and CV represents the seeding depth coefficient of variation, %.

3.2.3 Analysis of field test results

From the field test data (Table 3), the active control method shows significant advantages in peanut seeding depth control. Whether combining different operating speeds (3-5 km/h) with different seeding depths (40-60 mm), the active control method demonstrates the following strengths: The average seeding depth is closer to the preset value. The seeding depth qualification rate is higher. The standard deviation and coefficient of variation of seeding depth are smaller, indicating lower data dispersion and better stability.

Table 3 Field test results

Operating speed/ km·h⁻¹	Seeding depth/ mm	Seeding depth control method	Average seeding depth/ mm	Seeding depth qualification rate/%	Seeding depth standard deviation/ mm	Seeding depth coefficient of variation/ %
3	40	Mechanical	46.38	89.5	5.14	11.08
		Passive	47.22	90.7	4.38	9.28
		Active	40.73	93.2	3.05	7.47
	50	Mechanical	46.14	90.2	4.68	8.54
		Passive	46.63	91.5	4.24	9.09
		Active	50.11	94.8	3.12	6.08
	60	Mechanical	54.32	88.4	4.95	9.11
		Passive	55.35	89.2	3.49	6.31
		Active	58.62	93.6	3.48	5.94
4	50	Mechanical	46.35	85.6	5.49	11.36
		Passive	46.71	86.4	5.12	10.96
		Active	48.64	91.6	3.56	7.32
5	50	Mechanical	40.25	80.8	7.62	18.93
		Passive	41.23	81.6	6.37	15.45
		Active	45.62	86.4	5.84	12.80

Although the seeding depth control effect of all methods decreases as the operating speed increases, the active control method is less affected. It can still maintain good performance during high-speed operations and adapt well to different seeding depth requirements. Overall, its performance is far superior to that of mechanical control and passive control.

4 Conclusions

1) By building a system that uses ultrasonic sensors and displacement sensors to collect data collaboratively, this study obtains real-time seeding depth through height difference. Combined with the MLE-KF algorithm, it realizes adaptive filtering of measurement noise covariance, which effectively solves the problem that traditional Kalman filtering relies on prior knowledge of noise and is difficult to adapt to complex field environments.

2) This research takes the 1 MB-2/4 peanut film-laying seeder as the carrier, establishes a dynamic mathematical model of "frame height - push rod length - seeding depth", and uses an electric push rod to drive the parallel four-bar linkage to adjust the up and down movement of the furrow opener.

3) In the field test at the test base in Laixi City, Shandong Province, compared with traditional mechanical adjustment and passive profiling adjustment, the MLE-KF+fuzzy PID active control method in this study shows significant advantages. Under the working condition of an operation speed of 3 km/h and a set seeding depth of 50 mm, the seeding depth qualification rate reaches 94.8%. Even when the operation speed is increased to 5 km/h, the seeding depth qualification rate of active control can still maintain 86.4%. It is less affected by speed than traditional methods, meets the agronomic requirements of shallow peanut seeding, and has stronger stability and adaptability.

Acknowledgements

This study was supported by the National Key R&D Program Project (Grant No. 2023YFD2001002), the Doctoral Fund Project of Qingdao Agricultural University (Grant No. 663-1122016), and the Horizontal Research Project (Grant No. 660-2424484).

[References]

[1] Fang Z, Liu P L. Source of China's three major oilseeds production capacity improvement. Chinese Journal of Oil Crop Sciences, 2025; 47(2): 243-259. (in Chinese)

[2] Zhang L F, Lu J M, Zhang Y S, Shu X X, Chen X Y, Liu J, et al. Integrated application of green and efficient production technology for characteristic peanut in Yunnan. Chinese Journal of Oil Crop Sciences, 2024; 46(3): 536-543. (in Chinese)

[3] Wan S B, Zhang J L, Gao H X, Wang C B. Advances and prospects of high-yield peanut cultivation in China. Acta Agronomica Sinica, 2025; 51(7): 1703-1711. (in Chinese)

[4] Zhen X Y, Yang J Q, Li X X, Liu Z X, Gao F, Zhao J H, et al. Effects of sowing depth on growth process and leaf senescence of peanut and its physiological mechanism. Acta Agronomica Sinica, 2019; 45(9): 1386-1397. (in Chinese)

[5] Zhu R Y, Zhao M J, Yao Y F, Dong Y J, Hu G Q, Li X D, et al. Effects of straw returning methods and sowing depth on physiological characteristics of summer direct-seeding peanut seedlings. Chinese Journal of Oil Crop Sciences, 2024; 46(3): 507-517. (in Chinese)

[6] Wang Q Y, Xu Q M, Lu C Y, Li H W, He J, Wang Q J. Research status and development of key intelligent technologies for no-tillage seeding. Journal of South China Agricultural University, 2021; 42(6): 27-35. (in Chinese)

[7] Zhao J H, Liu L J, Yang X J, Liu Z J, Tang J X. Design and laboratory test of furrow opener depth control system for planter. Transactions of the CSAE, 2015; 31(6): 35-41. (in Chinese)

[8] Gao Y Y, Zhai C Y, Yang S, Zhao X G, Wang X, Zhao C J. Development of CAN-based downforce and sowing depth monitoring and evaluation system for precision planter. Transactions of the CSAM, 2020; 51(6): 15-28. (in Chinese)

[9] Zhao J L, Zhu L T, Jia H L, Huang D Y, Guo M Z, Cong Y J. Automatic depth control system for a no-till seeder. Int J Agric & Biol Eng, 2018; 11(1): 115-121.

[10] Wang S, Yi S, Zhao B, Li Y, Li S, Tao G, Mao X, Sun W. Sowing depth monitoring system for high-speed precision planters based on multi-sensor data fusion. Sensors, 2024; 24(19): 6331.

[11] Zhou L M, Ma Y H, Zhou H Y, Niu K, Zhao B, Wei L G, et al. Design and test of sowing depth measurement and control system for no-till corn seeder based on integrated electro-hydraulic drive. Applied Sciences, 2023; 13(10): 5823.

[12] Suomi P, Oksanen T. Automatic working depth control for seed drill using ISO 11783 remote control messages. Computers and Electronics in Agriculture, 2015; 116: 30-35.

[13] Iqbal T, Ghaffar A M, ur Rehman U, Saeed Y, Aqib M, Iqbal F, Saleem S R. Development of real time seed depth control system for seeders. Environmental Sciences Proceedings, 2022; 23(1): 7.

[14] Kim Y S, Kim T J, Kim Y J, Lee S D, Park S U, Kim W S. Development of a real-time tillage depth measurement system for agricultural tractors: Application to the effect analysis of tillage depth on draft force during plow tillage. Sensors, 2020; 20(3): 912.

[15] Nielsen S K, Munkholm L J, Lamandé M, Nørremark M, Edwards G T C, Green O. Seed drill depth control system for precision seeding. Computers and Electronics in Agriculture, 2018; 144: 174–180.

[16] Nielsen S K, Nørremark M, Green O. Sensor and control for consistent seed drill coulter depth. Computers and Electronics in Agriculture, 2016; 127: 690–698.

[17] Lyu J Q, Yang X H, Feng X, Li Z H, Li J C, Liu Z Y Design and experiment of sowing depth control device of potato planter. Transactions of the CSAE, 2020; 36(12): 13-21. (in Chinese)

[18] Xue B, Zhou L M, Niu K, Zheng Y K, Bai S H, Wei L A. Sowing depth control system of wheat planter based on adaptive fuzzy PID. Transactions of the CSAM, 2023; 54(S1): 93–102. (in Chinese)

[19] Wang C. Design of seeding depth adjustment system for planter based on PLC control. Journal of Agricultural Mechanization Research, 2019; 41(8): 105–109. (in Chinese)

[20] Pontin M, Colombo F, Mazza L, Raparelli T. Design and study of a pneumatically actuated inverted pendulum system controlled using a programmable logic controller. Proceedings of the Institution of Mechanical Engineers, Part I: Journal of Systems and Control Engineering, 2020; 234(7): 1023–1036.

[21] Zhao N, Zhao B, Yi S, Zhou Z, Che G. Research on a sowing depth detection system based on an improved adaptive Kalman filtering method. Electronics, 2022; 11(22): 3802.

[22] Li M W, Xia X M, Zhu L T, Zhou R Y, Huang D Y. Intelligent sowing depth regulation system based on Flex sensor and Mamdani fuzzy model for a no-till planter. Int J Agric & Biol Eng, 2021; 14(6): 145-152.

[23] Li Y Y, Qi B, Bao E C, Tang Z, Lian Y, Sun M Y. Design and analysis of a sowing depth detection and control device for a wheat row planter based on fuzzy PID and multi-sensor fusion. Agronomy, 2025; 15(6): 1490.

[24] Cao X P, Wang Q J, Xu D J, Huang S H, Wang X H, Wang L B. Design and analysis of pneumatic downforce regulating device for no-till corn planter. Agriculture, 2022; 12(10): 1513.

[25] Li B S, Tan Y, Chen J, Liu X X, Yang S H. Precise active seeding downforce control system based on fuzzy PID. Mathematical Problems in Engineering, 2020; 2020: 5123830.

[26] Liu W, Bian X, Deng Z, Mo J, Jia B. A novel carrier loop algorithm based on maximum likelihood estimation (MLE) and Kalman filter (KF) for weak TC-OFDM signals. Sensors, 2018; 18(7): 2256.

[27] Xu P, Kou J, Wang M, Tu T, Chen X, Luo J, Hu J, Lei X. Soil moisture detection and linear deceleration control strategy enhancing trenching depth precision and stability for rapeseed sowing. Agriculture, 2024; 14(10): 1717.

[28] Gao Y Y, Zhai C Y, Yang S, Zhao X G, Wang X, Zhao C J. Measurement method and mathematical model for the seeding downforce of planter row unit. Transactions of the CSAE, 2020; 36(5): 1–9. (in Chinese)

[29] Foster J, Bevis M, Businger S. GPS meteorology: Sliding-window analysis. Journal of Atmospheric and Oceanic Technology, 2005; 22(6): 687–695.

[30] Chhabra A, Venepally J R, Kim D. Measurement noise covariance-adapting Kalman filters for varying sensor noise situations. Sensors, 2021; 21(24): 8304.

[31] GB-T6973-2005. Test methods for single seeder (precision seeder). Machinery Industry Publishing House, Beijing, China, 2005. (in Chinese)